Journal of Solid State Chemistry 241 (2016) 173–179

Contents lists available at ScienceDirect

Journal of Solid State Chemistry

journal homepage: www.elsevier.com/locate/jssc

On the electrical properties of the $Bi_{2-y}Sr_yIr_2O_7$ pyrochlore solid solution: Quantum *ab initio* and classic calculations

Pablo de la Mora [a,b,*], Carlos Cosio-Castañeda [c], Oliver Martinez-Anaya [c], Francisco Morales [d], Gustavo Tavizon [c]

[a] Mechanical Engineering, University of Texas at Austin, TX, USA
[b] On sabbatical leave from Departamento de Física, Facultad de Ciencias, UNAM-CU (Universidad Nacional Autónoma de México, Ciudad Universitaria, México, D.F. 04510, MEXICO)
[c] Departamento de Física y Química Teórica, Facultad de Química, UNAM-CU
[d] Instituto de Investigaciones en Materiales, UNAM-CU

ARTICLE INFO

Article history:
Received 23 December 2015
Received in revised form
10 June 2016
Accepted 11 June 2016
Available online 14 June 2016

Keywords:
Pyrochlore iridiate
$Bi_2Ir_2O_7$
Electrical resistivity of iridiates
Bi-iridiates

ABSTRACT

In this work, a theoretical study of the electrical properties of the $Bi_{2-y}Sr_yIr_2O_7$ ($Bi_{2-y}Sr_yIr_2O1_6O2$) α-pyrochlore-type solid solution is presented. Quantum *ab initio DFT*(*WIEN2k*) calculations were performed in order to understand the electrical resistivity changes associated to the Bi substitution by Sr in this system. The main crystallographic modification associated to this substitution is the x position of the 48*f* oxygen (x, $\frac{1}{8}$, $\frac{1}{8}$) (O1); this substitution substantially modifies the Bi/Sr–O1 and Ir–O1 atomic distances, increasing the former and diminishing the latter. Experimentally, the $Bi_{2-y}Sr_yIr_2O_7$ samples are metallic and the electrical resistivity increases with the Sr content. Electronic structure calculations for $Bi_2Ir_2O_7$ and $BiSrIr_2O_7$ show that, regardless of structural changes, there is only a small change of electrical conductivity with the Sr substitution, and the experimentally observed increase of the resistivity can be explained in terms of a larger impact on the electronic structure of both; the Sr 'impurities' as well as of the thermal Sr oscillations.

1. Introduction

Transition metal oxides adopting the crystal structure of α-pyrochlore show a wide variety of physical phenomena such as colossal magnetoresistance [1], metal-insulator transitions [2,3], and a complex magnetic behavior that arises from the non-collinear geometric arrangements of the magnetic moments. More recently a topological insulator behavior has been suggested for the $A_2Ir_2O_7$ system (A=Y or rare-earth element) [4,5]. Physical properties exhibited by α-pyrochlores have introduced new concepts in condensed matter physics as order-by-disorder [6,7], spin ice [8–11], cooperative paramagnetism [12], and others [13]. Magnetic oxides crystallizing in the pyrochlore crystal structure represent a kind of intriguing system in which their magnetic behavior is strongly dependent of the geometric arrangement of the magnetic moments, where magnetic frustration and non-collinearity of the magnetic moments play an important role [14]. Despite this complexity, several α-pyrochlore systems have been used in oxygen reduction reactions as electrocatalysts substituting Pt [15,16], solid oxide fuel cell electrodes [17], and as a thermal barrier coating [18,19].

Electronic conductivity of the pyrochlore oxides, $A_2M_2O_7$ (M is a 3*d*, 4*d* or 5*d* transition metal), has been understood in terms of the t_{2g}-block bandwidth and factors that can modify the overlap between the *d*-metal and the 2*p*-oxygen orbitals (the *M*–O and *A*–O distances and the *M*–O–*M* angle) [20]. Using this criterion, contrary to the experimental measurements, the $Bi_2Ir_2O_7$ pyrochlore is expected to be a better conductor than $Bi_2Ru_2O_7$ [20–24]. This difference remarks the importance of understanding the electrical properties of 4*d*- and 5*d*-metal oxide systems, associated to their band structure. In this regard, $Bi_2Ru_2O_7$ and $Bi_2Ir_2O_7$, both of them metallic and isostructural, are different; the metallic behavior of the former originates from the extended character of the Bi–6*p* band [25,26], whilst in the latter the metallic state arises from the Ir–O1 sublattice [27].

Considering the *A* cations in the $A_2Ir_2O_7$ system, when *A*=Gd, Tb, Dy, Ho, Yb and Y, these pyrochlores exhibit a semiconducting behavior, while for *A*=Pr, Nd, Sm and Eu, they were found to exhibit metallic behavior [3]. Particularly, when the 4*f* *A*-cations are involved in the crystal structure, and due to their localized character, only the 5*d*–Ir and 2*p*–O1 electrons are responsible for the electronic conductivity. An especial situation results with *A*=Nd,

* Corresponding author.
E-mail address: delamora@unam.mx (P. de la Mora).

http://dx.doi.org/10.1016/j.jssc.2016.06.013
0022-4596/

Sm, and Eu, in which a second-order metal-insulator (M-I) transition occurs [15]. The lanthanide contraction plays an important role and as the *A* cation becomes smaller, the Ir–O distance increases and the 5*d*-2*p* overlap is smaller, the t_{2g} bandwidth becomes narrower and eventually the compounds become insulators [2,28].

Early experimental studies on the $R_2Mo_2O_7$ (*R*=rare-earth element) pyrochlore showed good correlation between the R^{3+} radius, the crystallographic cell constant and the insulating or metallic character of this series [3]. In addition, ferromagnets were found to be metallic while paramagnets were insulating [29,30]. Electrical behavior of $R_2Ir_2O_7$ is closely related with the overlap between the Ir–5*d* and the O–2*p* orbitals, and in this way the metal-insulator transition can be intuitively explained in terms of the *R* ionic size [3]. The same situation seems to appear in the $A_2Mo_2O_7$ system that shows a M-I transition as a function of the A^{3+} ionic radii [29]. On the basis of single-crystal measurements, Qi et al. [31] have suggested the existence of an exotic ground state for $Bi_2Ir_2O_7$. Electronic properties of this system and other iridiates as $Na_4Ir_3O_8$ have recently attracted much attention [32–34] due to their intriguing properties.

Band structure calculations on the $A_2Ir_2O_7$ system have shown that the crystal field effect associated with the *A*-site ion plays an important control parameter for the M-I changeover [25]. As previously shown [27], there exists a deviation from the ideal (undistorted) IrO_6 octahedron crystal field splitting for Ir^{4+}, but the system preserves its original metallic character due to the wide bands. The main contribution to the density of states at the Fermi energy (E_F) comes from the Ir_2O1_6 sublattice, this assertion is valid in the $0 \le y \le 1$ range. However, the experimental electrical resistivity of samples does depend on, and increases with, the Sr content [27]. Our aim in this work is to provide an explanation of the experimental electrical resistivity behavior of the $Bi_{2-y}Sr_yIr_2O_7$ solid solution [27]. This explanation is given by means of electronic structure calculations, and the thermal vibrations of atoms by a simple harmonic oscillations model of springs and masses.

2. Calculation details

Electronic structure calculations on the $Bi_{2-y}Sr_yIr_2O_7$ ($y=0, 1$) systems were done with the *WIEN2k* code [35]. *WIEN2k* is a full potential-linearized augmented plane wave (*FP – LAPW*) method based on Density Functional Theory (*DFT*). The generalized gradient approximation of Perdew et al. [36] was used for the treatment of the exchange-correlation interactions. For the number of plane waves the used criterion was R_{MT}^{min} (muffin tin radius) $\times K^{max}$ (for the plane waves)=9. The number of *k*-points used was $10 \times 10 \times 10$. The energy convergence criterion was 10^{-4} Ry.

In the relaxation time approximation framework, the electrical conductivity ($\sigma_\alpha = 1/\rho_\alpha$, in the α direction, where ρ is the resistivity) is [37–39].

$$\sigma_\alpha = (e^2/\hbar\Omega)\tau \int \nu_\alpha dA_\alpha = \frac{\tau\omega_p^2}{4\pi}, \quad (1)$$

where ν_α is the electron velocity ($=1/\hbar \; d\varepsilon/dk_\alpha$, the last term, $d\varepsilon/dk_\alpha$, is the slope of the band, and is evaluated at $\varepsilon=E_F$), A_α is the area perpendicular to ν_α, Ω is the volume of the unit cell, τ is the relaxation time, ω_p is the plasma frequency and it can be calculated with the *WIEN2k* (using the OPTIC and JOINT subprograms), but for this calculation a much finer mesh, $27 \times 27 \times 27$, is needed ([40] Section 8.17). The integral of Eq. (1) contains the terms that are related to the band structure of the ideal crystal. The relaxation time, τ, introduces the effect of the 'imperfections' of the crystal, i.e., the more imperfections, the shorter τ is. In turn, τ has two terms that contribute in the following way [38].

$$1/\tau = 1/\tau_d + 1/\tau_{ph}, \quad (2)$$

where τ_d is due to defects. The other term, τ_{ph}, is the phononic contribution due to the thermal oscillations of the atoms; these oscillations increase with temperature, thus τ_{ph} is shortened. In terms of the resistivity there are two corresponding terms:

$$\rho = 1/\sigma = \rho_d + \rho_{ph}. \quad (3)$$

3. Results and discussion

In the $A_2Ir_2O_7$ pyrochlore, $A=Bi_{2-y}Sr_y$ (Fig. 1A), there are two substructures of tetrahedra, $Ir_{4/2}O1_6$ and $A_{4/2}O_2$ (Ir and *A* are shared between two tetrahedra, Fig. 1(B) and (C)). Each of these substructures forms the three dimensional version of the Kagome structure. At the center of the two Ir tetrahedra there is an iridium atom surrounded by six oxygen atoms forming a distorted octahedron $IrO1_6$, which can also be seen as a trigonal antiprism. This antiprism changes with doping, from a flattened for $Bi_{2-y}Sr_yIr_2O_7$, $y=0$ ($Bi_2Ir_2O1_6O2$), where the O^a–Ir–O^b angle (O^a and O^b belong to different tetrahedra, see central Ir in Fig. 1(C)) is $\theta \sim 83°$, to an elongated one for $y=0.9$, with $\theta \sim 97°$ [27]. For an intermediate

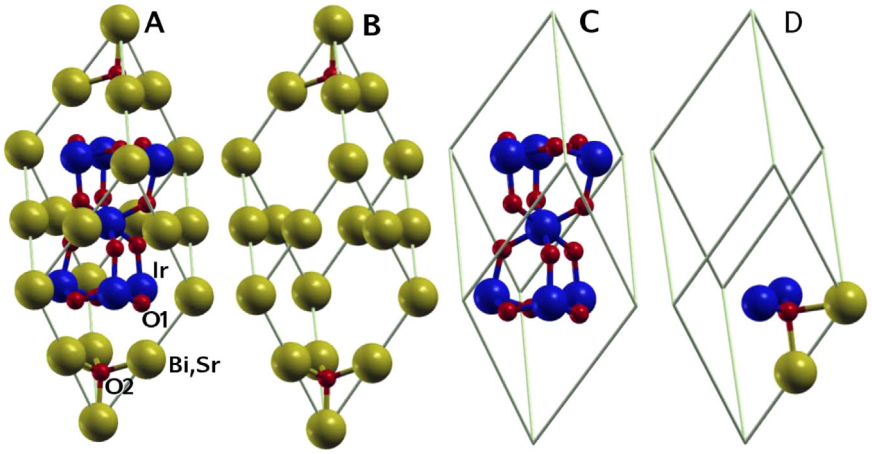

Fig. 1. (A) Primitive cell of the crystal structure of α-pyrochlore, $A_2B_2O1_6O2$ (which contains two formula units, in this case $Bi_2Ir_2O1_6O2$ ($\times 2$), Bi is partially substituted by Sr). (B) A_2O2 ($\times 2$) sublattice (C) Ir_2O1_6 ($\times 2$) sublattice. (D) *A*–Ir tetrahedron (*A*–O1 bonds were added for clarity). The positions of the atoms were shifted by 1/2, 1/2, 1/2 so that the Ir_4O1_6 tetrahedra and the $IrO1_6$ trigonal antiprism would be clearly visible.

composition, y~0.5, $IrO1_6$ would form an undistorted octahedron (θ~90°). This trigonal antiprism deformation is claimed to lead to topological insulator behavior [4,5] in $Y_2Ir_2O_7$, but the present system exhibits wide bands and this deformation has little effect.

Although O1 is in the Ir tetrahedra, O1 is also inside of a tetrahedron made of two *A* and two Ir atoms (see Fig. 1(D)). As previously reported [27], O1 moves towards the Ir atom as a function of the Sr content. This is consistent with a theoretical structure-property model made by Koo et al. [20]. In their paper, they argue that in each mixed A_2B_2O tetrahedron, as those present in the pyrochlore structure, when *A* (Bi) is replaced by a larger cation, such as Sr, the oxygen atom, O1, moves towards the other cation *B* (Ir). The Bi^{3+} and Sr^{2+} ionic radii (CN=8) are 1.17 Å and 1.26 Å, respectively [41].

Besides the structural distortion, the substitution of Bi^{3+} by Sr^{2+} is supposed to change the oxidation state of Ir^{4+}, to maintain the electroneutrality of the $Bi_{2-y}Sr_yIr_2O_7$ system. On the other hand, there is the possibility to generate some oxygen vacancies [42,43].

In the ruthenium pyrochlores $Bi_{2-x}Ln_xRu_2O_7$ (*Ln*=Pr-Lu) [24], a M-I transition is observed as function of the x composition ($x \simeq 1.2 - 1.4$) and of the crystallographic parameters [26]. For the metallic systems, $A_2Ru_2O_7$, A=Tl^+, Pb^{2+} and Bi^{3+}, the main structural difference with those nonmetallic compounds is the Ru–O1 bond-distance value (less than 2.00 Å), and the Ru–O1–Ru angle ($\theta > 132.5°$) [26], larger than the observed in the semiconducting oxides. However, in Ir pyrochlores the thermal variation of the resistivity has been associated to the ionic radius and the lattice parameter. For metallic Ir pyrochlores, the ionic radius of the *A* atom needs to be larger than 1.08 Å and the lattice parameter larger than 10.25 Å [2,3]. In a previous work, we have shown that for the metallic $Bi_{2-y}Sr_yIr_2O_7$ system the electrical resistivity is an almost linear function of the Ir–O1 bond distance [27]. What is puzzling in this system is that the resistivity increases with the shortening of the Ir–O1 bond, which is the opposite trend observed in the above-mentioned ruthenates.

Fig. 2 shows the resistivity measurements as a function of temperature (ρ *vs.* T) of the $Bi_{2-y}Sr_yIr_2O_7$ system. These measurements and sample preparation were previously reported [27]. The resistivity measurements were performed in sample bars of $5 \times 2 \times 2$ mm^3 using the four-probe method, the applied current was 10 mA. The measurements were performed into a closed-cycle cryocooler. $\rho(T)$ curves show an almost linear behavior with a positive slope ($d\rho/dT > 0$). This, in terms of electronic structure, means that there is no gap in the density of states at E_F. In this system, both the resistivity and its slope increase with the Sr content. As the Sr content increases there is a shortening of the Ir-O1 bond distance (Fig. 1(D)) and the O^a–Ir–O^b angle also increases [27]. The conductivity is expected to increase, which is contrary to the observed trend in the experimental measurements. As mentioned above, in pyrochlore ruthenates the conductivity indeed increases.

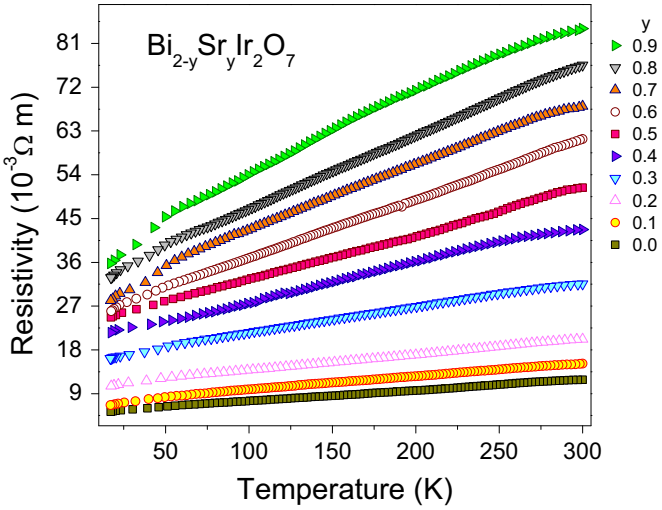

Fig. 2. Temperature dependence of the experimental electrical resistivity for the $Bi_{2-y}Sr_yIr_2O_7$ compounds, with $0.0 \le y \le 0.9$ [27]. Note that the residual resistivity and the $\rho(T)$ slope increase with the Sr content in all samples.

To analyze these experimental results for the $Bi_{2-y}Sr_yIr_2O_7$ system, electronic structure calculations were done for (A) y=0 ($Bi_2Ir_2O_7$, 'Bi_2', with cell parameter a=10.3121 Å, where the distance of O1 from the center of the tetrahedron is x=0.206 cell units (cu)) and (B) y=1 ($BiSrIr_2O_7$, 'BiSr' a=10.3336 Å, O1: x=0.183 cu), this is an extrapolation from the y=0.9 experimental case [27]. In the last system, half of the Bi atoms are substituted by Sr, this should have been done in a random way. To model this, a large supercell would be needed (the primitive cell has 22 atoms), and the calculation would be quite computer-consuming, specially for the electrical conductivity calculations. For these reasons the substitution was done in the primitive cell. As it will be seen below, the Bi_2O2 subsystem contributes little to the *DOS* at E_F (inset of Fig. 3B), and the Bi-Sr ordering would weakly affect the bands in this energy region; then two of the Bi atoms, among the four in the primitive unit cell, were replaced by Sr. This substitution reduces the cubic symmetry SG 227 (F d-3m) to tetragonal SG 74 (I mma) and now the z axis is not equivalent to the x and y axes. It also implies two modifications, on one hand, the charge distribution associated to the chemical substitution of Bi^{3+} by the larger Sr^{2+} and, on the other hand, the change of crystal cell parameters due to this substitution.

The calculations were initially spin polarized with spin-orbit (SO) coupling correction. The SO mixes the up/down bands and the number of bands in the band-structure doubles, although in the present case the magnetic moment is very small and the band splitting is $\sim 10^{-3}$ eV, then the calculations were non spin polarized.

For the 'Bi_2' system, the band structure (Fig. 3(A)) shows four bands near E_F, with an apparent gap at -0.5 eV and a large gap at 1.2 eV above E_F. Three bands cross E_F and the compound is a conductor. The slope of the bands is proportional to the conductivity (Eq. (1) and following), and it can be seen that most of the bands have a large slope at E_F. The Density of States (*DOS*, Fig. 3 (B)) shows that the main contribution at E_F is due to the Ir and O1 atoms, with a small contribution from Bi and O2. In other words, the Bi_2O2 sublattice contribution to the *DOS* is quite small (1/10 compared with the Ir_2O1_6 sublattice). On the other hand (Fig. 4A), the 'BiSr' system has a band structure with similar slopes at E_F, which is the relevant part for the electrical conductivity, although the apparent gap below E_F disappears and the gap above E_F becomes an apparent gap. In this case the BiSrO2 sublattice contributes even less (1/50 compared with the Ir_2O1_6 sublattice).

We can observe (Fig. 5), in going from 'Bi_2' to 'BiSr', that one half of the Bi^{3+} are substituted by the larger Sr^{2+}, thus Sr^{2+} pushes O1 towards Ir (see the A_2Ir_2O1 tetrahedron in Fig. 1(D)) shortening the Ir–O1 bond. As can be observed from the band structure results, the bands at E_F are more separated, but the slope of the bands is similar. As a consequence, the electronic part of the conductivity, $\int v_\alpha dA_\alpha$, would be expected to be similar for both compositions.

To investigate the effect of the Bi substitution by Sr on the conductivity of the $Bi_{2-y}Sr_yIr_2O_7$ system, two intermediate compounds were calculated: 'Bi_2-near' and 'BiSr-far' (Fig. 5). (1) 'Bi_2-near', in which only the crystal cell parameters are modified but Bi is not replaced by Sr, i.e., 'Bi_2' is now calculated with the 'BiSr'

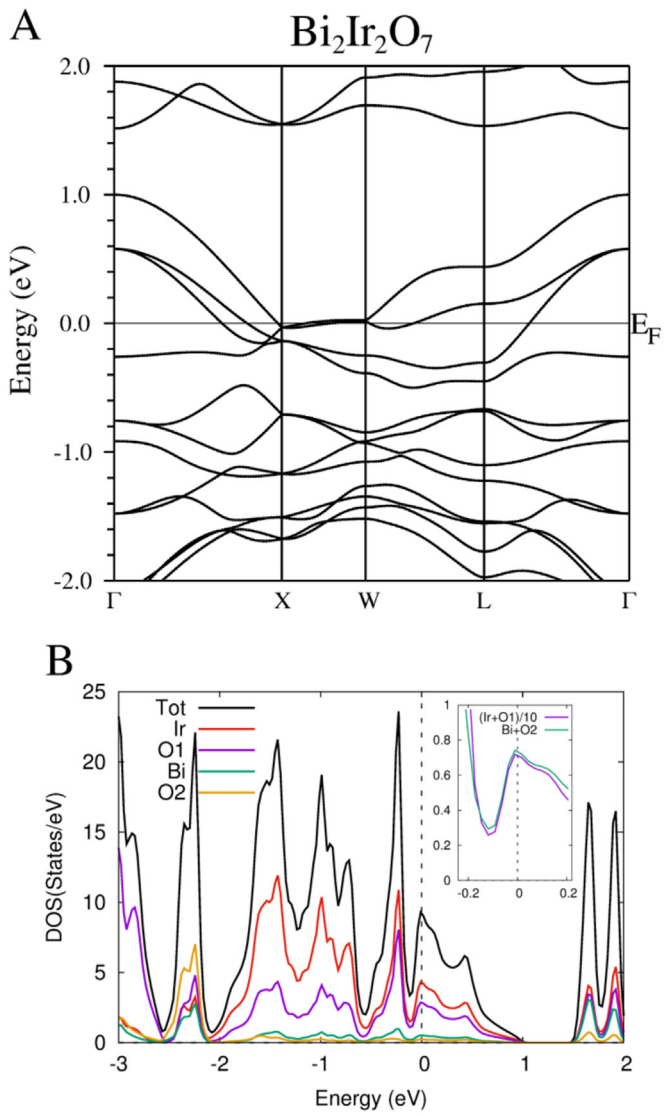

Fig. 3. (A) Band structure and B) density of states of $Bi_2Ir_2O_7$, 'Bi_2'. From these figures, it can be observed that the compound is metallic with three bands crossing E_F. In the inset of panel B, the Ir+O1 and Bi+O2 contributions are compared; as it can be seen Bi+O2 contributes very little and the conductivity is mainly in the Ir+O1 substructure.

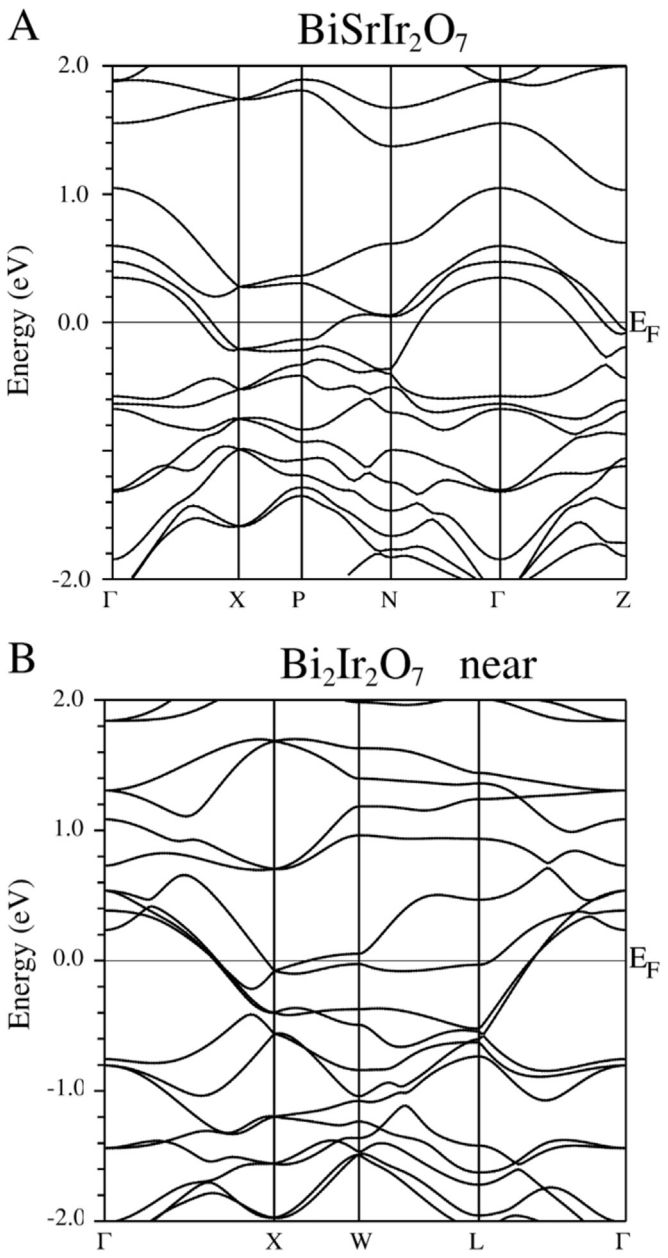

Fig. 4. Band structure of, (A) 'BiSr', the larger Sr atom enlarges the cell, but the bandwidths and the number of bands crossing E_F remain the same, the symmetry now is not the same as in 'Bi_2' Γ-X splits into Γ-X and Γ-Z, for this reason the path Γ-X-P-N-Γ in 'BiSr' is an equivalent path to Γ-X-W-L-Γ in 'Bi_2', although it is not the only one. (B) 'Bi_2-near', due to the higher overlap of Ir–O1, the bands widen; four bands cross E_F and the electronic component of the conductivity should increase.

crystal cell parameters. In this intermediate compound, the crystal cell parameters change only slightly (0.2% larger), but more importantly, the O1 is considerably closer to Ir: 2.01 Å for 'Bi_2' and 1.87 Å for the 'BiSr' case (7.5% shorter). (2) In 'BiSr-far', 'BiSr' is now calculated with the 'Bi_2' crystal cell parameters.

In 'Bi_2-near', O1 has a larger Ir–O1 overlap compared with 'Bi_2', which gives wider bands (Fig. 4(B)), this is difficult to see in Γ-X since these wider bands now cross between them, but in L-Γ it is clearer, a band that goes from −0.3 to +0.56 in 'Bi_2', now it goes from −0.56 to +0.56 in 'Bi_2-near'. As a consequence of the larger width, there is a larger slope at E_F. Additionally, four bands, instead of three, cross E_F. These two facts should give a higher conductivity. When we substitute one-half of Bi by Sr in the 'Bi_2-near' compound, then 'BiSr' is obtained. What could be expected is that the bands would remain rather unchanged, but E_F would shift downwards. What we observe is that in the 'BiSr' compound the bands become narrow again (Fig. 4(A)).

The reason to introduce 'Bi_2-near' and 'BiSr-far' is to separate (a) the effect of the Ir–O bond shortening and (b) the Bi chemical substitution by Sr on the electronic structure and in the conductivity. The electronic calculations of these two systems are expected to dilucidate the two types of contributions to the electric conductivity in Eq. (1): those resulting from the relaxation time effect, τ, and those from the electronic part, $I = (e^2/\hbar\Omega)\int \nu_\alpha dA_\alpha = \omega_p^2/4\pi$.

To quantify these changes, the electronic part of the conductivity equation, I, was calculated. The results are shown in Table 1.

There is a correspondence between I and the widths of the bands plus the number of bands crossing E_F. When going from 'Bi_2' to 'BiSr', the bandwidths are almost the same and there is only a moderate increase in I of 1.49, that is, the electronic resistivity is reduced by 33%. This change in resistivity is associated only with the effect of the chemical substitution of Bi by Sr.

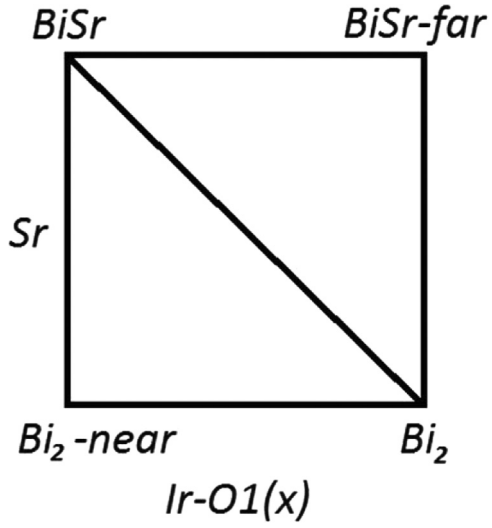

Fig. 5. Diagram of the modifications in the $Bi_{2-y}Sr_yIr_2O_7$ system that result from the structural changes of the *Bi* substitution. Going to the right, the Ir–O1 distance is increased (x); going up, Bi is replaced by Sr keeping x constant. To go from 'Bi_2' ($Bi_2Ir_2O_7$) to 'BiSr' ($BiSrIr_2O_7$) one has to go up and left. In the diagonal are the experimental compounds, while in the two other corners are two hypothetical compounds; 'Bi_2-near' ('Bi_2' with 'BiSr' parameters) and 'BiSr'-far' ('BiSr' with 'Bi_2' parameters).

Table 1
Electronic part of the conductivity, $4\pi I$ ($=\omega_p^2$), calculated for the four systems considered: Bi_2, Bi_2-near, BiSr and BiSr-far.

Compound	ω_p^2 (eV^2)
Bi_2	3.0974
Bi_2-near	7.5627
BiSr	4.6082
BiSr-far	1.4295
	$4\pi I$ ratio
BiSr/BiSr-far	3.2237
Bi_2-near/Bi_2	2.4416
BiSr/Bi_2	1.4877

In the first step of Fig. 5, in going from 'Bi_2' to 'Bi_2-near', there is a large increase in the bandwidths and the number of bands crossing E_F goes from 3 to 4; I increases by a factor of 2.44. This is the effect of the Ir–O1 bond shortening. On the other hand, going from 'BiSr' to 'BiSr-far', there is a larger reduction in I of 1/3.22. That is, the overall effect of increasing the Ir-O1 bond distance is that I is 32% larger in 'BiSr' than in 'Bi_2'.

The main structural change in going from 'Bi_2' to 'Bi_2-near' and in going from 'BiSr-far' to 'BiSr' is the movement of O1 towards the Ir atom (Fig. 1(D)), and this can be taken as an estimate of the effect of atomic vibrations on the electronic structure. In the first case, 'Bi_2-near' to 'Bi_2', the I ratio is 2.44, while in the second case, 'BiSr' to 'BiSr-far', it is 3.22; and this can be interpreted as the Ir–O1 vibrations having a larger effect on the electronic structure of 'BiSr' than on that of 'Bi_2'. These results show that the electronic part of the conductivity, I (see Table 1), goes in the opposite direction of the experimental results (see Fig. 2); I has only a little increase as a consequence of the Bi substitution by Sr. Observing Eq. (1), one reasonable origin of the decrease of conductivity σ_α (increase of the resistivity, ρ_α) is the reduction of the relaxation time, τ (Eqs. (1) and (2)), associated to the crystal imperfections linked to the Bi substitution by Sr.

With respect to the effect of the crystal imperfections, the Bi by Sr replacements can be regarded as impurities or crystal imperfections, but these are in the A_2O2 sublattice. This sublattice contributes little to the density of states (Fig. 3(B)) and as a consequence, this Bi by Sr replacement by itself should affect little the conductivity, which is contrary to the observed experimental results (Fig. 2). The effect of this replacement on the electrical resistivity can be understood in an indirect way: Sr perturbs O1 of the Ir_2O1_6 sublattice. This perturbation has two components: one static, in which the larger Sr ion pushes O1 towards Ir, and one dynamic, in which the O1 oscillations perturb differently when Bi is replaced by Sr. These two contributions have a large effect on the band structure (Figs. 3(A) and 4(A) show the effect of replacing Bi by Sr, Figs. 3(A) and 4(B) shows the effect of moving O1 in 'Bi_2'). The static term of resistivity, ρ_d, increases the resistivity at $T=0$ K; and the dynamic one, ρ_{pH}, increases the slope (Fig. 2) of the resistivity. With these two terms we will be able to explain the observed temperature dependence of electrical resistivity of the $Bi_{2-y}Sr_yIr_2O_7$ system.

The static effect, when Bi is replaced by Sr, the electronic part of the resistivity decreases by 33%, but this replacement introduces impurities in the otherwise 'perfect' crystal, which would have zero resistivity. This replacement has two effects; (a) Sr is larger than Bi, which displaces O1 towards Ir, and (b) Sr has lower charge than Bi. These two factors affect the Ir_2O1_6 sublattice, since the Sr replacement is expected to occur in a random way, this introduces disorder in the Ir_2O1_6 sublattice, reducing τ_d (increasing ρ_d, Eq. (3)), this term corresponds to the residual resistivity ($T=0$), due to defects in the lattice. In this way ρ_d increases with the Bi replacement by Sr.

The dynamic effect, when a lighter atom as Sr replaces Bi, it has larger dynamic oscillations at a given temperature. These oscillations increase with temperature and the slope of the temperature dependence of resistivity, $d\rho/dT$, also increases.

With a simple model, it will be shown that not all the Sr oscillations are larger than those of Bi, but, acting as impurities, the overall effect will be that the oscillations in 'BiSr' will have a larger dynamic contribution than in 'Bi_2'.

The dynamics of the Bi/Sr oscillations in the pyrochlore system could be studied with the package phonopy [44], which is quite computer demanding, even more for a Bi/Sr random supercell. Instead, a simple and linear model of spring and masses will be used. In the $Bi_{2-y}Sr_yIr_2O_7$ crystal structure, either Bi or Sr (M_i) are surrounded by oxygen atoms, O, and around these there are Ir and other M_i atoms (Fig. 1). This is a complicated system, but what is important are the oscillation amplitudes of Bi/Sr and the surrounding oxygen atoms. This will be studied with a linear model in which Bi/Sr has O in each side, and these O are connected to the rest of the crystal by a spring; here the 'rest' will be taken as static,

$$|-O-M_i-O-|,$$

where '–' represents a spring, and at the end the springs are fixed to a wall '|'. In this model, the two oxygen atoms will be assumed to move in the same direction; when the oxygen atoms move in opposite directions M_i remains static and would not represent a dynamic perturbation. Although this model is very simple, it gives a good idea of the relative amplitudes of the thermal oscillations of M_i and O. This system can be solved for harmonic oscillations, $x_i = A_i\cos(\omega t)$, where x_i are the atomic displacements. These oscillations are due to thermal perturbations, i.e., at a given temperature the average energy of each oscillation mode should be the same, therefore the relative amplitudes are given for constant energy of the whole spring-masses system.

There are two vibrational modes, one is the acoustic mode, in which M_i and O move in the same direction; and the other one is

Table 2
Relative oscillation amplitudes of atoms in the $| - O - Mi - O - |$ model, here the spring constant is taken as $k=1$.

Mode	System	Amplitude		
		M_i	O	M_i–O distance
Acoustic	Bi-O	1.413	0.733	0.680
	Sr-O	1.408	0.768	0.640
Optic	Bi-O	0.054	−0.680	0.734
	Sr-O	0.128	−0.640	0.768

Table 3
M_i – O amplitudes in the $| - O - Mi - O - |$ model, with the calculated spring constants (the % are calculated with respect to 'Bi_2').

	'Bi_2'	'BiSr'			
	Bi-O	Bi-O		Sr-O	
Acoustic	7.271	7.467	2.7%	7.390	1.6%
Optic	7.849	8.061	2.7%	8.862	12.9%

the optical mode, in which M_i and O move in opposite directions. The relative amplitudes of these oscillations, with the same spring constant ($k=1$), are given in Table 2.

The spring constants k are different and they can be estimated by making small displacements, δ, of the atoms, which increase the total energy of the system. From the classic E *vs.* δ curve the spring constant can be obtained. In 'Bi_2' the 'Bi–O' constant can be estimated by making small displacements of Bi, and in 'BiSr' the 'Bi–O' and 'Sr–O' spring constants can be estimated by displacing Bi and Sr respectively. These constants were found to be 0.00873 in 'Bi_2', 0.00828 for 'Bi–O' and 0.00751 for 'Sr–O' in 'BiSr'. With these spring constants the amplitudes are modified. Table 3 shows the modified M_i – O amplitudes.

The M_i – O oscillations in the 'BiSr' system are moderately larger than in the 'Bi_2' system. In the acoustic mode this distance barely changes when Bi is replaced by Sr, while for the optic mode there is a 13% increase for the Sr sites. This is a surprising result given the large mass difference between Bi and Sr ($M_{Bi}/M_{Sr}=2.39$); on the other hand, O is much lighter ($M_{Sr}/M_O=5.48$) and all the energy goes to the heavy atom and the O oscillations remain fairly unchanged. The small increment of amplitudes, Table 3, with the Bi by Sr replacement does not totally explain the increase of resistivity.

The experimental increase in resistivity could be explained as follows. When half of the Bi is replaced by Sr in 'Bi_2' to obtain 'BiSr' two aspects can be considered, (a) the Sr^{2+} is distributed in a random way that creates local static perturbations, these reduce τ_d (Eqs. (1)–(3)) and increase the residual resistivity (see Fig. 2, 'BiSr' has a residual resistivity 8 times larger than 'Bi_2'). (b) There are also atomic oscillations, phonons, which cause dynamic perturbations ($1/\tau_{ph}$). Now, as mentioned above, with the Bi by Sr substitution the atomic displacements have a larger effect on the electronic structure (see Table 1). That is, the electrons would collide, scatter, more often by the impurities, τ would be shortened more in 'BiSr' than in 'Bi_2', as a consequence, when temperature increases the oscillation amplitudes also increase and the slope of the resistivity as a function of temperature, $d\rho/dT$, in 'BiSr' would be larger than in 'Bi_2'. In this way, the increment in resistivity, which goes in the opposite direction of the electronic component of the conductivity equation (Eq. (1)), can be explained as the effect of the Bi substitution by Sr on resistivity, that should be associated to the change on the relaxation time. This is due to the compositional disorder and to the stronger effect of the Sr–O oscillations on the electronic structure that reduce τ more than the Bi–O oscillations.

4. Conclusions

The electrical resistivity measurements of the $Bi_{2-y}Sr_yIr_2O_7$ system as a function of the Sr content can be explained in terms of Eqs. (1) and (2). The electrical resistivity has two contributions; the electronic component ($1/\omega_p{}^2$) and that of the impurities that are included in τ. The electronic component of resistivity is reduced by 33% as Bi is substituted by Sr in $Bi_2Ir_2O_7$, which is contrary to the experimentally observed results. This can be explained as the result of the shortening of the relaxation time, τ, which would increase the resistivity. Sr replaces Bi in the real crystal, acting as an impurity; the introduction of Sr has no direct influence in the electronic structure since the A_2O2 sublattice does not significantly contribute to DOS, but it affects indirectly the Ir_2O1_6 sublattice. This modification is the main responsible for the changes of the electronic conductivity. The relaxation time has two components, 1) one static due to impurities, and in this case the resistivity at $T=0$ K increases with the Sr content; and 2) one dynamic due to the oscillations of O1; this is because the Sr oscillations affect the Ir_2O1_6 sublattice more than those of Bi. The difference between the Bi and Sr contributions to the oscillations explains the slope of the resistivity *vs.* temperature behavior.

Acknowledgements

The authors would like to thank Sabina Ruiz–Chavarría and Juan Manuel Rámirez de Arellano for computer support and Sra. Claudia Rosas for technical support. Financial support from PAPIIT (UNAM; Universidad Nacional Autónoma de México, Mexico) under projects IN-113913, IN-223515 and PAIP-FQ (UNAM) is also acknowledged. P. de la Mora thanks the Programa de Apoyos para la Superación del Personal Académico de la UNAM.

References

[1] A.P. Ramirez, J. Phys. : Condens. Matter 9 (1999) 8171–8199.
[2] K. Matsuhira, M. Wakeshima, Y. Hinatsu, S. Takagi, J. Phys. Soc. Jpn. 80 (2011) 094701.
[3] D. Yanagishima, Y. Maeno, J. Phys. Soc. Jpn. 70 (2001) 2880–2883.
[4] B.J. Yang, Y.B. Kim, Phys. Rev. B 82 (2010) 085111.
[5] X. Wan, A.M. Turner, A. Vishwanath, S.Y. Savrasov, Phys. Rev. B 83 (2011) 205101.
[6] S.T. Bramwell, M.J.P. Gingras, J.N. Reimers, J. Appl. Phys. 75 (1994) 5523–5525.
[7] J.D.M. Champion, M.J. Harris, P.C.W. Holdsworth, A.S. Wills, G. Balakrishnan, S. T. Bramwell, E. Cizmar, T. Fennell, J.S. Gardner, J. Lago, D.F. McMorrow, M. Orendac, A. Orendacova, D.M. Paul, R.I. Smith, M.T.F. Telling, A. Wildes, Phys. Rev. B 68 (2001) 020401.
[8] P.W. Anderson, Phys. Rev. 102 (1956) 1008–1013.
[9] M. Harris, S. Bramwell, D. McMorrow, T. Zeiske, K. Godfrey, Phys. Rev. Lett. 79 (1997) 2554.
[10] A.P. Ramirez, A. Hayashi, R.J. Cava, R. Siddharthan, B.S. Shastry, Nature 399 (1999) 333–335.
[11] S.T. Bramwell, M.J. Gingras, Science 294 (2001) 1495–1501.
[12] J.S. Gardner, S.R. Dunsiger, B.D. Gaulin, M.J.P. Gingras, J.E. Greedan, R.F. Kiefl, M. D. Lumsden, W.A. MacFarlane, N.P. Raju, J.E. Sonier, I. Swainson, Z. Tun, Phys. Rev. Lett. 82 (1999) 1012–1015.
[13] A. Keren, J.S. Gardner, G. Ehlers, A. Fukaya, E. Segal, Y.J. Uemura, Phys. Rev. Lett. 92 (2004) 107204.
[14] S.S. Sosin, L.A. Prozorova, M.R. Lees, G. Balakrishnan, O.A. Petrenko, Phys. Rev. B 82 (2010) 094428.
[15] T. Konishi, H. Kawai, M. Saito, J. Kuwano, H. Shiroishi, T. Okumura, Y. Uchimoto, Top. Catal. 52 (2009) 896–902.
[16] J. Prakash, D.A. Tryk, W. Aldred, E.B. Yeager, J. Appl. Electrochem. 29 (1999) 1463–1469.
[17] P. Holtappels, J. Bradley, J.T.S. Irvine, A. Kaiser, M. Mogensen, J. Electrochem. Soc. 148 (2001) A923.
[18] L. Liu, Q. Xu, F. Wang, H. Zhang, J. Am. Ceram. Soc. 91 (2008) 2398–2401.

[19] X. Cao, R. Vassen, W. Fischer, F. Tietz, W. Jungen, D. Stöver, Adv. Mater. 15 (2003) 1438–1442.
[20] H. Koo, M.H. Whangbo, B.J. Kennedy, J. Solid State Chem. 136 (1998) 269–273.
[21] M. Tachibana, Y. Kohama, T. Shimoyama, A. Harada, T. Taniyama, M. Itoh, H. Kawaji, T. Atake, Phys. Rev. B 73 (2006) 193107.
[22] H. Fukazawa, Y. Maeno, J. Phys. Soc. Jpn. 71 (2002) 2578–2579.
[23] R.E. Carbonio, J.A. Alonso, J.L. Martínez, J. Phys. Condens. Matter 11 (1999) 361–369.
[24] T. Yamamoto, R. Kanno, Y. Takeda, O. Yamamoto, Y. Kawamoto, M. Takano, J. Solid State Chem. 109 (1994) 372–383.
[25] F. Ishii, T. Oguchi, J. Phys. Soc. Jpn. 69 (2000) 526–531.
[26] M. Field, B. Kennedy, B.A. Hunter, J. Solid State Chem. 151 (2000) 25–30.
[27] C. Cosio-Castaneda, P. de la Mora, G. Tavizon, J. Solid State Chem. 184 (2011) 1251–1256.
[28] K. Matsuhira, M. Wakeshima, R. Nakanishi, T. Yamada, A. Nakamura, W. Kawano, S. Takagi, Y. Hinatsu, J. Phys. Soc. Jpn. 76 (2007) 043706.
[29] J. Greedan, M. Sato, N. Ali, W. Datars, J. Solid State Chem. 68 (1987) 300–306.
[30] N. Ali, M. Hill, S. Labroo, J. Greedan, J. Solid State Chem. 83 (1989) 178–187.
[31] T.F. Qi, O.B. Korneta, X. Wan, L.E. DeLong, P. Schlottmann, G. Cao, J. Phys. Condens. Matter 24 (2012) 345601.
[32] L. Balents, Nature 464 (2010) 199–208.
[33] Y. Okamoto, M. Nohara, H. Aruga-Katori, H. Takagi, Phys. Rev. Lett. 99 (2007) 137207.
[34] M.J. Lawler, A. Paramekanti, Y.B. Kim, L. Balents, Phys. Rev. Lett. 101 (2008) 197202.
[35] P. Blaha, K. Schwarz, G.K.H. Madsen, D. Kvasnicka, J. Luitz, An Augmented Plane Wave+Local Orbitals Program for Calculating Crystal Properties, 2001.
[36] J.P. Perdew, K. Burke, M. Ernzerhof, Phys. Rev. Lett. 77 (1996) 3865–3868.
[37] P. de la Mora, M. Castro, G. Tavizon, J. Phys. Condens. Matter 17 (2005) 965–978.
[38] N. Ashcroft, N.D. Mermin, Solid State Physics, Holt-Saunders International Editions, London, 1976.
[39] P.B. Allen, W.E. Pickett, H. Krakauer, Phys. Rev. B 37 (1988) 7482–7490.
[40] P. Blaha, K. Schwarz, G. Madsen, D. Kvasnicka, J. Luitz, User's Guide, WIEN2k 14.2 (Release 10/15/2014), Techn. Universitat Wien Institut fur Physikalische und Theoretische Chemie, Wien/Austria, 2014.
[41] R.D. Shannon, Acta Crystallogr. Sect. A 32 (1976) 751–767.
[42] C. Cosio-Castaneda, P. de la Mora, F. Morales, R. Escudero, G. Tavizon, J. Solid State Chem. 200 (2013) 49–53.
[43] B. Kennedy, J. Solid State Chem. 123 (1996) 14–20.
[44] A. Togo, I. Tanaka, First principles phonon calculations in materials science, Scr. Mater. 108 (2015) 1–5.